Soft Matter

PAPER

View Article Online
View Journal | View Issue

Cite this: *Soft Matter*, 2016, **12**, 1621

Dynamics of colloids confined in microcylinders

S. Ghosh, D. Wijnperlé, F. Mugele and M. H. G. Duits*

Received 18th October 2015,
Accepted 24th November 2015

DOI: 10.1039/c5sm02581h

www.rsc.org/softmatter

We studied both global and local effects of cylindrical confinement on the diffusive behavior of hard sphere (HS) colloids. Using confocal scanning laser microscopy (CSLM) and particle tracking, we measured the mean squared displacement (MSD) of 1 micron sized silica particles in water–glycerol. This combination of fluid and setup allowed us to measure MSDs in a 4-dimensional parameter space, defined by the HS volume fraction (Φ: 0.05–0.39), cylinder radius (R: 2.5–20 micron), distance to the wall (z) and lagtime (τ: 0.03–60 s). MSDs for the entire cylinder confirm earlier findings that both narrowing the cylinder and populating it cause a slower dynamics. Additionally a decrease in R was found to cause a stronger ordering of the fluid. The effect of confinement on dynamics was further examined as a function of (z) location. For the largest cylinder (with minor curvature), we found that the strong decrease in MSD near the wall, becomes much less pronounced for higher Φ. Analyzing the radial (r) and azimuthal (θ) components, we found pronounced differences in the z-dependence that were 'hidden' in the total MSD. Near the wall, the r-MSD shows a much steeper z-dependence while at larger z, it shows a remarkable anti-correlation with the (peaked) density $n(z)$. Also the dependence of the r-MSD on lagtime correlates with $n(z)$: diffusive in between layers, but subdiffusive inside layers. These observations bring earlier findings together, while also shedding new light on the diffusive dynamics of concentrated colloids in narrow capillaries.

1 Introduction

Dynamics of colloids in confinement is of interest for both fundamental and practical reasons as the boundary and size-effects can alter the material properties[1–3] and relaxation time(s)[4–6] (*e.g.* glass forming liquids) of a suspension, which in turn can influence the transport mechanism through narrow cavities.[7,8] Confinement induced changes in dynamics can also be accompanied by alterations in the local structure of the fluid.[5] When subjecting a confined suspension to flow, both the structure and the dynamics are modified;[9–12] this is of relevance to micro- and nanofluidics[13] and nanotribology.[14]

The present study is focused on the diffusive dynamics in the quiescent state. The simplest way to provide confinement here, is *via* a single hard wall. Already this can significantly alter the dynamics of the colloids *via* potential (*i.e.* thermodynamic) and hydrodynamic interactions (HI). Slow-down of particle motion near a flat wall has been observed for several systems at low particle concentrations. Extensions to the case of a curved wall have been explored, but the conditions where curvature starts to play an important role, have not been mapped out in a systematic manner. Further extending from a curved wall to a full cylinder produces a new case, since besides the curved interface, also the overall confinement will influence the dynamics. For a large cylinder radius (relative to the particle size), the interfacial effect should be similar to that of a single flat wall. However on making the cylinders progressively narrower, a transition from a local to a global confinement should be expected. Also the particle volume fraction should play a role here, considering that the structure and dynamics generally become more strongly transmitted at higher concentrations. However, so far no systematic studies into the combined effects of cylinder radius and particle volume fraction have been done, not even for the case of hard spheres and hard walls.

The key role of particle volume fraction in the dynamics of confined systems is well established, and clear distinctions can be made between the dynamic regimes at different volume fractions. At low concentrations where the particles behave almost independent of each other, effects are mainly observed close to the wall(s), where displacements towards or away from the wall are strongly opposed by hydrodynamic forces. At higher concentrations but still below the HS glass transition, hydrodynamic interactions between the particles modulate the effect of walls.[15] Not only the volume fraction but also the structure in the fluid then plays a role. At the very high concentrations of glass forming liquids, drastic slowdown of the diffusive dynamics has been associated with correlated motions[16,17] that become noticeable when the length scale of

Physics of Complex Fluids Group, Department of Science and Technology, MESA+ Institute for Nanotechnology, University of Twente, P.O. Box 217, 7500 AE Enschede, The Netherlands. E-mail: m.h.g.duits@utwente.nl

confinement becomes comparable to the cooperative length scale.[18] Also studies of colloidal suspensions in (quasi-) 2D systems[19–25] have demonstrated dynamical heterogeneities. Differences in particle mobility[26] may or may not be caused by differences in local structure.

But in spite of these significant insights, much is still unknown about how confinement changes the (diffusive) dynamics. While the dilute limit has been considered theoretically[27,28] and experimentally[29–34] by several researchers, and the same for the glassy state,[6,35,36] for intermediate particle concentrations results are relatively scarce. In this regime, the diffusive dynamics is a result of an interplay between structure and hydrodynamics, where both are influenced by the confining walls.

Studies on the diffusive dynamics of moderately concentrated suspensions near a flat wall with light scattering[15,37–39] showed that the wall effect gradually diminishes with increasing particle concentration. However optically no distinction could be made between different distances from the wall. It is therefore still not settled how the wall effect on particle dynamics is transmitted to the interior of the suspension and to what extent the influence will remain significant. In confinement by more than one wall, both the dimensionality and shape of the confining geometry also play a role. Confinement by two parallel walls[19–21,23,35,40] provides a simple case, where particle motion was found to be restricted towards the wall. Confinement in an almost cylindrical capillary was considered for a binary suspension.[41] Recently, also an extension was made to the role of the mechanical properties (softness or fluidity)[42,43] of the confining material.

In this work we consider the case of hard sphere colloids confined by cylindrical hard walls. Based on the reviewed literature, two general trends are expected also in our case: (i) narrowing down the confinement should lead to a slower (average) dynamics of the particles. This slowing down should become more drastic at higher volume fraction. (ii) confining walls have a layering effect, *i.e.* the highest local concentration of particles should occur at the wall. Specific new aspects that will be considered here, are: (1) the transition from the local confinement by one wall, to a global one that corresponds to the entire cylinder, (2) the dependence of this transition on particle volume fraction and (3) local variations in the dynamics, considering both the distance from the wall, and the (radial and azimuthal) directionality of the motion and (4) the role of local particle concentration on the dynamics.

2 Experiments

2.1 Sample preparation

We synthesized[44–46] core–shell silica spheres of 1.0 μm diameter (polydispersity ≈ 5%) containing a core of 500 nm diameter labelled with Fluorescein isothiocyanate (FITC) to allow detection of the centre of mass of each particle accurately, even at high concentrations. These colloidal probes were suspended in water–glycerol mixture (18 : 82 by weight, mass density $\rho_s = 1.21$ g ml^{-1}) to achieve near refractive index matching with the silica spheres ($n_p = 1.46$), thus minimizing the scattering of light. Suspensions of different volume fractions were prepared by diluting a stock solution with volume fraction (Φ) = 0.45. The method of the sample preparation is described in ref. 10. We also added LiCl to the suspension (up to 0.8 mM) to screen the surface charge; the corresponding calculated electrical double layer thickness[47] of about 8 nm should be sufficiently small to make a nearly HS system in water–glycerol. The theoretical settling speed of the silica spheres (mass density $\rho_p = 1.89$ g ml^{-1}) is less than 10 nm s^{-1} in the dilute limit, and expectedly about 10 times slower at $\Phi \approx 0.3$.[48] Considering the height of the cylinders (24 μm) and the total time lapse between the filling of the channel and the last experiment (800 s), this means that changes in suspension concentration (at the focal plane) can be neglected. Five particle volume fractions (Φ = 0.05, 0.28, 0.32, 0.35 and 0.39) were prepared.

2.2 Microfluidics

Microcylinders of different diameters were designed embedded in the side walls of the microchannels as shown in Fig. 1a. Molds made from SU8 were fabricated on silicon wafers by soft lithography, and subsequently transferred to channels by negative stamping in poly(dimethylsiloxane) (PDMS). We mainly used 30 μm (width) × 24 μm (height) × 1 cm (length) PDMS channels bonded onto a 170 μm thick glass cover slip, after making them hydrophilic using Oxygen plasma for 50 s at 100 W. Since the hydrophilicity of the PDMS can last for nearly 200 h,[49] and sticking of particles onto the channel walls had to be avoided, we waited at least 2 weeks before using the channels. Both ends of the microchannel were connected with reservoirs to allow pressure control without problems due to solvent evaporation. The connections between the microcylinders and the channel consisted of rectangular necks with a length of at least 10 μm and a width of 3 μm (smallest cylinder) to 6 μm (largest cylinder); these dimensions were appropriate to ensure absence of flow inside the cylinders during the measurements. Cylinders were filled directly with the suspension. As soon as the particles had reached the outlet, the second reservoir was connected, the hydrostatic pressures were balanced, and a waiting time of 5 min was given. Fig. 1b shows a snap shot of a microcylinder filled with the silica spheres. All experiments were performed at 22 ± 1 °C.

2.3 Imaging by confocal microscopy

We use a VisiTech 'VT-infinity^3' Confocal Laser Scanning Microscope (CSLM) to visualize the motion of the colloids. The microscope is connected to a Hamamatsu digital camera (ORCA-flash 4.0) and a 488 nm laser source. To obtain the best spatial resolution for particle localization, we used a 100× oil immersion objective with 1.3 numerical aperture. This resulted in a field of view of 65 μm × 75 μm and an effective pixel size of 130 nm. The focal plane was set at the mid plane (H = 12 μm) of the microchannel structure, to minimize the influence of the top and bottom walls on the particle dynamics. Considering the finite field of view, cylinders were recorded one by one, except the smallest two which were imaged simultaneously. For each

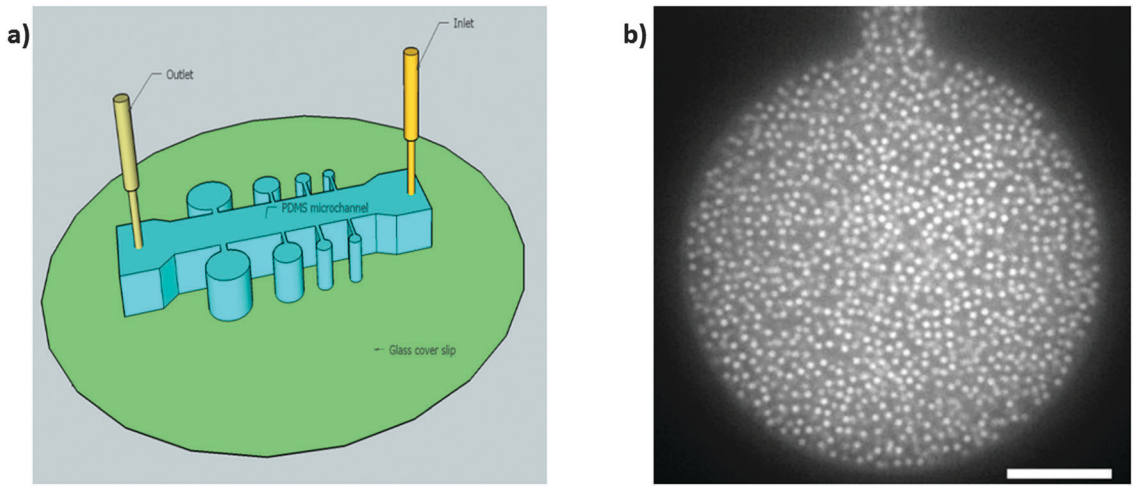

Fig. 1 (a) Schematic of the experimental setup. Microcylinders are embedded in the side of the microchannel of 1 cm length, 30 μm width and 24 μm height. Diameters are 40 μm, 20 μm, 10 μm and 5 μm. (b) Confocal image of a suspension at volume fraction 0.28, taken 12 μm above the bottom. Scale bar: 10 μm.

concentration, typically 5000 frames were recorded at a rate of 30 fps. The total number of trajectory steps varied from 4×10^5 ($\Phi = 0.05$, $R = 2.5$ μm) to 6×10^6 ($\Phi = 0.39$, $R = 20$ μm). We also imaged the suspensions in bulk at the same concentration and height inside a large holder, *i.e.* without confinement.

3 Data analysis

Standard particle tracking software[50,51] was used to localize and track particles. Since our video recordings had a duration of ≈150 s per cylinder, and the particle dynamics needed to be precisely resolved with respect to distance from the wall, correction for table drift was essential.[9] The average drift velocity (calculated from particle trajectories) was typically 2 nm s^{-1}, corresponding to a total cylinder displacement of ≈300 nm per recording. Over plotting the (drift corrected) particle coordinates of the entire movie resulted in images like Fig. 2a and b. Measuring the axis location (and radius) of the cylinder from the contour allowed a coordinate transformation from (x, y) to (r, θ) for each particle position: $r^2 = x^2 + y^2$ and $\theta = \tan^{-1}(y/x)$, where the centre of the cylinder was taken as the origin ($x = 0$, $y = 0$).The availability of θ coordinates was then used to exclude all particles with θ values that occurred within 15 degrees from the neck of the cylinder. The remaining data were used to assess the accuracy in the measured cylinder radius, by inspecting $r(\theta)$ plots as in Fig. 2c. Depending on the particle volume fraction and cylinder radius, the inaccuracy varied between 0.5 and 1.0 pixel (65–130 nm), *i.e.* about 2 times the standard deviation of the particle size distribution. Since r corresponds to the radial position of a particle centre, the physical radius R of the cylinder was obtained by adding one particle radius (500 nm) to the 'maximum detected radius' indicated by the dashed line in Fig. 2c.

3.1 Concentrations

Local particle concentrations were calculated as a function of r by counting the number of detected particles in a ring

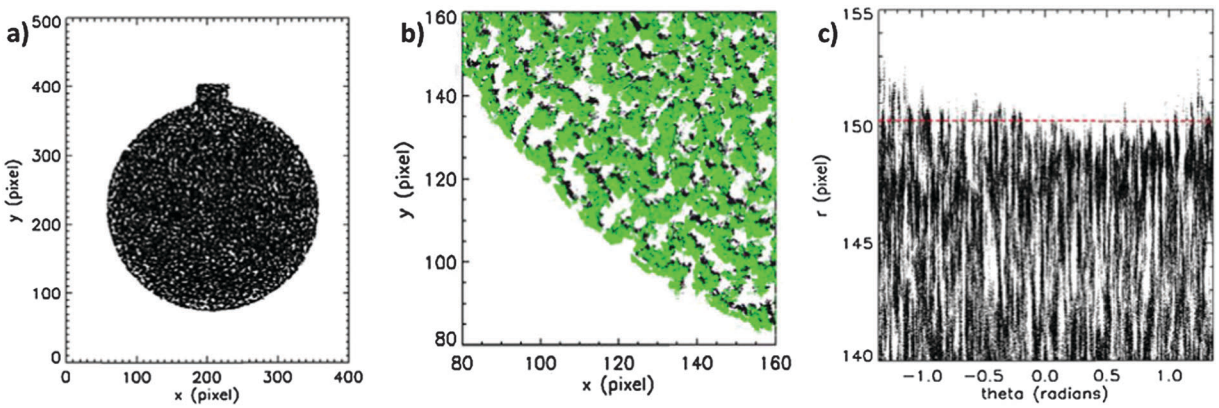

Fig. 2 Measurement of the center location and radius of the cross section of the cylinder, for the experiment at $\Phi = 0.28$ and $R = 20$ μm. (a) time projection of all (drift corrected) particle center coordinates. (b) Zoom in, also comparing the non-corrected (black) and drift-corrected (green) coordinates. (c) Same data as in (b) but now plotted as r *vs.* θ. The neck occurring around $\theta = \pi/2$ has been left out.

with radius r and width dr and normalizing for the area of the ring:

$$n(r) = N_p(r) \Big/ \left[(\theta_{max} - \theta_{min}) \left(r + \frac{1}{2} dr \right) dr \right] \qquad (1)$$

where $N_p(r)$ is the number of particles found within dr and θ_{min}, θ_{max} indicate the angular range over which was integrated. dr is the width of the r-bin, which was set equal to 50 nm. The angular range between 75° to 105° which corresponds to the neck area, is excluded from the calculation. It should be noted that N_p depends on the selection criteria used in the preceding image analysis step. Accordingly, in our 3D system where the distance of a particle to the focal plane follows a distribution, the measured number of particles per unit area $n(r)$ does not have a simple meaning. However, given that the illumination conditions and camera settings were the same, $n(r)$ should be proportional to the local volume fraction.

3.2 Mean squared displacements

In the calculations of spatially resolved MSDs, the transformation to polar coordinates was applied to the center of mass (x_{CM}, y_{CM}) of each trajectory, after which r_{CM} was used to assign a specific r-bin to the considered trajectory. For all particle volume fractions and cylinder radii, the total r-range was binned with a Δr of 0.13 μm. Considering that the typical MSD at a lagtime of 100 s lies between 0.01 and 0.1 μm^2 (see Fig. 4), this choice should be appropriate: although some particles visited other r-bins than they were assigned to, the ensuing 'smearing' of the r-dependent MSDs should be small.

Decomposition of the (local) MSDs in the radial (r) and azimuthal (θ) directions was done using the θ coordinate of the center-of-mass of each individual trajectory. Using this θ_{CM}, each individual displacement (vector) $\Delta\vec{s}$ of the particle was split into Δs_r and Δs_θ: $\Delta s_\theta = \Delta\vec{s}\cdot\vec{e}_\theta$ and $\Delta s_r = \Delta\vec{s}\cdot\vec{e}_r$ with $\vec{e}_r = \cos\theta_{CM}\,\vec{e}_x + \sin\theta_{CM}\,\vec{e}_y$ and $\vec{e}_\theta = -\sin\theta_{CM}\,\vec{e}_x + \cos\theta_{CM}\,\vec{e}_y$.

Here $\vec{e}_r$ is the unit vector in the direction of r_{CM}, while $e\&\vec{e}_\theta$ points in the perpendicular direction that makes θ increase. $\vec{e}_x$ and $\vec{e}_y$ are the unit vectors in the x and y directions. While this decomposition ensures that the length of $\Delta\vec{s}$ is conserved in all coordinate transformations (also the ones involving multiple steps), some 'cross-bleeding' between the displacements in the r and θ directions occurs, if the average location of the particle in the given displacement step, does not fall on the line that runs through the origin (*i.e.* the center of the circle) and (x_{CM}, y_{CM}). This error, which is illustrated in Fig. 3, is largest near the origin, where the distinction between r and θ directions is least important. Close to the wall, the error is small.

Mean squared displacements (for an individual trajectory) in the r and θ directions were then calculated after introducing new arrays to represent the (lag)time dependent displacement of a single particle i:

$$S_r(i,j) = S_r(i,0) + \sum_{k=1}^{j} \Delta s_r(i,k) \quad \text{for} \quad j = 1 \text{ to } N_j \qquad (2)$$

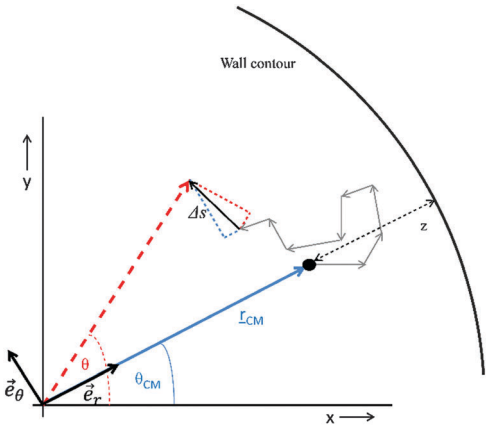

Fig. 3 Illustration (not to scale) of the approximation made in the decomposition of individual displacements into radial and azimuthal directions. r_{CM} and θ_{CM} indicate the center-of-mass location of a trajectory (most steps of which are not shown). Individual displacement steps Δs (like the one in black) are decomposed into the radial and azimuthal directions, belonging to r_{CM} (dotted blue lines). The actual r and θ displacements (red dotted lines) belonging to the red dashed lines are slightly different. z indicates the radial distance of centre of mass position from the wall. The black curve represents the wall contour.

$$S_\theta(i,j) = S_\theta(i,0) + \sum_{k=1}^{j} \Delta s_\theta(i,k) \quad \text{for} \quad j = 1 \text{ to } N_j \qquad (3)$$

where $S_r(i,0)$ and $S_\theta(i,0)$are arbitrary constants, j indicates the time (N_j is the number of steps of the trajectory). These new arrays were then analysed for the entire set of trajectories by the standard routine for calculating MSD (components),[51] as if they were x and y coordinates. Finally, for the purpose of analysing the MSDs as a function of distance to the wall (z), the r_{CM} label of each trajectory was transformed into a z-label *via* $z = R - r_{CM}$. Plotting MSDs *versus* z allows to compare between cylinders having different radii.

4. Results and discussion

4.1. Global MSDs

Lagtime-dependent MSDs were measured for 4 volume fractions (Φ = 0.05, 0.28, 0.35 and 0.39) and 5 degrees of confinement (R = 2.5, 5, 10, 20 μm and ∞, *i.e.* bulk fluid). The data for bulk fluids (shown in Appendix A) show similar behaviour to earlier findings for colloidal hard spheres:[17,19,52] on increasing Φ, the MSD gets smaller, while the lagtime dependence become subdiffusive. These changes in MSD magnitude and signature are minor at low Φ (<0.1) but show a strong dependence on volume fraction for $\Phi > 0.3$.

Increasing the confinement while keeping Φ constant, results in similar trends. As shown in Fig. 4, reducing R from ∞ to 2.5 μm has a modest effect on the MSD at Φ = 0.05, while at Φ = 0.39 the MSD clearly becomes sub-diffusive, especially for the two smallest R (intermediate volume fractions not shown). These MSDs are obtained from all trajectories, irrespective of their position inside the cylinders. Considering the data at Φ = 0.05, the MSDs of the bulk fluid show a remarkable difference

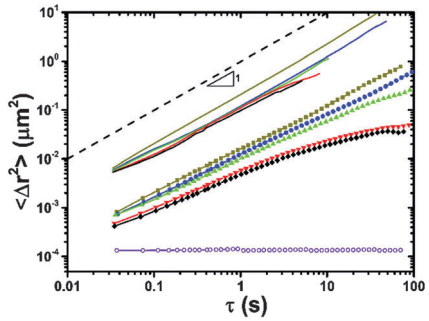

Fig. 4 Lagtime-dependent MSDs for bulk and confined fluids at different volume fractions Φ = 0.05: lines and Φ = 0.39: solid symbols. Cylinder diameters: 40 μm (blue); 20 μm (green); 10 μm (red); 5 μm (black). Dark yellow line and symbols represent bulk MSDs. MSDs for Φ = 0.05 have been multiplied with 5 for clarity. Dashed line is of slope unity and open circles (magenta) indicate the noise floor.

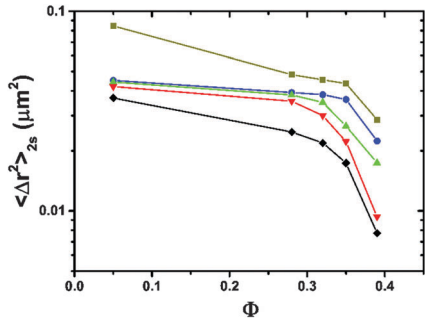

Fig. 5 Total MSD as a function of volume fraction confined in different cylinders. All MSDs are measured at τ = 2.0 s. Symbols for the different cylinder diameters (d_{cyl}): 40 μm (blue circle), 20 μm (green upper triangle), 10 μm (red lower triangle), 5 μm (black diamond). Dark yellow squares belong to the respective bulk MSDs.

with those of the confined fluids. This is ascribed to the strong local effect of the cylinder wall: in the limit of low Φ, a strong reduction in diffusion coefficient takes place in the first 2 particle layers near the wall.[29] These two layers makes a relatively strong contribution to the average MSD for the whole cylinder. As we will show, at Φ = 0.39 the effect of the nearby wall on the local MSD is less strong; this explains why at this volume fraction the data at R = 20 μm and those for $R \rightarrow \infty$ are closer to each other.

In Fig. 5 we illustrate these trends, by intersecting the data as in Fig. 4 at a representative lag time of 2 s, and plotting the MSD magnitude *vs.* volume fraction. Now including all Φ, we find that the effect of cylindrical confinement on the MSD is more drastic at higher volume fractions (taking into account the previous remark about the data point at Φ = 0.05). Also this trend corresponds well to earlier findings for colloidal HS, albeit that most of these were made in plate-plate geometries.[19,23] It thus appears that at the level of the total MSD (*i.e.* neither distinguishing between locations, nor between the directions of the diffusive motion), the difference between confinements by cylinders or by flat plates is modest.

In several previous studies, these trends were interpreted as 'confinement induced freezing'. While our experiments do not really reach the 'freezing' regime, the trends are similar to *e.g.* work of Eral *et al.*[19] who also found the beginning of sub-diffusive behaviour in bulk between Φ = 0.37 and 0.42, and significant confinement effects for $\Phi > 0.33$, leading to MSD plateaus under extreme confinement. An exploratory experiment performed by us at Φ = 0.45 and R = 2.5 μm also showed a lag-time independent MSD (data not shown). This gives further confirmation that 'confinement induced freezing' is also found in cylinders.

We extend our analysis by considering how the structure in the fluid is influenced by the confinement. Fig. 6a and b show how the number of particles per unit area depends on the distance to the cylinder wall, for different cylinder radii. For both Φ = 0.28 and 0.39 (and also at the intermediate Φ values), $n(z)$ shows a strong peak at the wall (regardless of cylinder radius). This observation agrees well with earlier theoretical[35,53–56] and experimental studies[23,57–59] where walls with a curvature radius much bigger (∞) than the particle radius, were found to have a strong layering effect. Also the increase in sharpness of the (first) concentration peak with the overall Φ corresponds with earlier findings.

Interestingly, the data in Fig. 6 also show a clear effect of increasing confinement on the structure of the fluid in the entire cylinder. As R is reduced, the $n(z)$ profiles become more pronounced, indicating that the ordering in the fluid increases. This is best visible in Fig. 6b for Φ = 0.39: the peaks in $n(z)$ get higher, while the minima become lower. For the two smallest cylinder radii, the ordering is even preserved over the entire

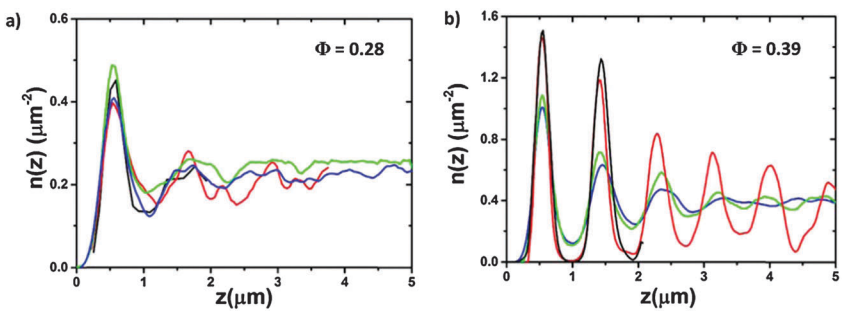

Fig. 6 Comparison of number density $n(z)$ as a function of distance from the wall for two representative volume fractions. Cylinder diameters: 40 μm (blue), 20 μm (green), 10 μm (red), 5 μm (black).

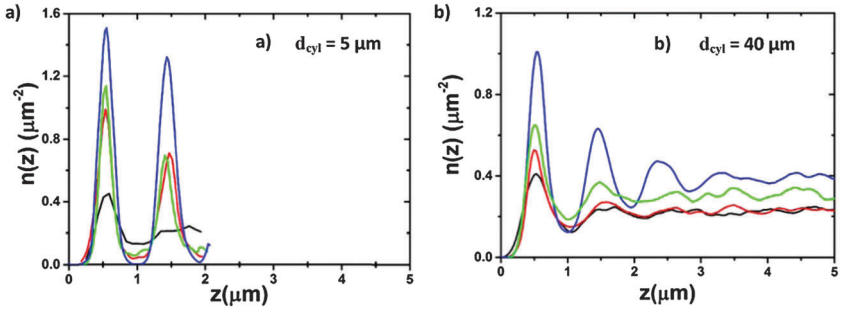

Fig. 7 Comparison of number density $n(z)$ as a function of distance from the wall for different concentrations (at fixed cylinder diameter). Volume fraction (Φ): 0.28 (black), 0.32 (red), 0.35 (green), 0.39 (blue).

z-range (while it vanishes at large z for the two largest cylinder radii). We remark that this confinement-induced 'transmission' of the order in the fluid, appears to be significantly stronger than in a previous study where two horizontal flat plates were used to confine the colloids.[19] This difference might be due to the alignment of the z-direction with gravity, and/or the fact that one wall had a significant roughness in the previous work (in the present study, the entire wall is smooth while the in-plane distribution of particles is not influenced by gravity).

Since the confinement-induced ordering might bear similarity to the effect of increasing the overall particle volume fraction, it is interesting to consider Fig. 7, which shows $n(z)$ for different Φ as a function of z for two representative cylinder radii. Even when taking into account that the peaks will be higher, partly because of the higher Φ, it is clear that the degree of order (the relative magnitudes of the maxima and minima of $n(z)$) is increased. The similarity between the effects of increasing confinement and increasing particle concentration on the structure in the fluid has not been demonstrated earlier as far as we know. It could indicate that (in our case) ordering plays a slightly different role in the slowing down of the particle dynamics *via* spatial confinement. The argument that spatial confinement shifts the glass transition to lower volume fractions is generally associated with the concept of hydrodynamic clusters, which does not assume a certain order.

4.2. Local MSDs

We now examine the effects of the spatial confinement on the MSD at different locations inside the cylinder. In previous works, diffusion coefficients (and for more concentrated systems MSDs) have been measured as a function of distance to the wall.[20] In the limit of low Φ, particle tracking experiments by Eral *et al.*[29] showed that their $D_r(z)$ and $D_\theta(z)$ that were similar to predictions by Brenner for a particle near a single flat wall.[27] Small differences could be attributed (almost quantitatively) to effects of wall curvature and the presence of end-surfaces. Michailidou *et al.*[15,38] studied more concentrated systems near a single wall, using a Dynamic Light Scattering technique. Our data allow extension of these works by measuring MSDs in concentrated fluids as a function of distance to the wall.

For R = 20 μm, the difference between MSD in the heart of the cylinder and the bulk MSD is modest. This suggests that close to one wall, the contributions of all other walls might be negligible. Since $R \approx 20a$ *i.e.* 20 times the particle radius, the curvature might be negligible, in which case we could almost translate the results to that of particles near single walls. Fig. 8 shows (for all Φ) the z-dependent magnitude of the MSD at a lagtime of 2.0 s; the choice for this lagtime is not critical, since the MSDs are still (nearly) diffusive for R = 20 μm (see Fig. 4). Comparison of the MSDs in the central area of the cylinder ($R > 3$ μm) with their corresponding values in bulk fluid, reveals that – except for Φ = 0.39 – the global effect of confinement is relatively small (compared to the changes in MSD as the wall is approached). This provides reasonable justification for comparing the results with the dynamics of suspensions near single (and flat) walls. In other words, neither the top and bottom surfaces, nor the curvature of the wall appears to play a role. Also the fairly close correspondence with the theoretical prediction of Brenner for a single particle corroborates this approach. We observe in Fig. 8 that as Φ is increased, both the structure in the MSD and the range over which it steeply decreases as the wall is approached, become smaller. This suggests a stronger hydrodynamic screening, *i.e.* in the particle dynamics the presence of the wall gets increasingly masked by the (dense suspension of) particles near the wall. Another observation in Fig. 8 is that whereas at low Φ the MSD increases gradually on moving away from the wall, as the volume fraction gets higher, also some 'structure' becomes visible in the z-dependent MSD. This aspect will be discussed in more detail below.

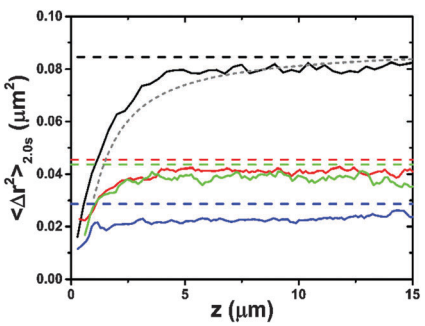

Fig. 8 Total MSD (at lag time 2.0 s) as a function of distance from the wall in fixed cylinder for various particle concentrations. Particle volume fractions (Φ): 0.05 (black), 0.32 (red), 0.35 (green), 0.39 (blue). Dotted grey line represents the theoretical prediction calculated from ref. 27 and 30. Dashed lines are the respective bulk MSD values. Cylinder radius = 20 μm.

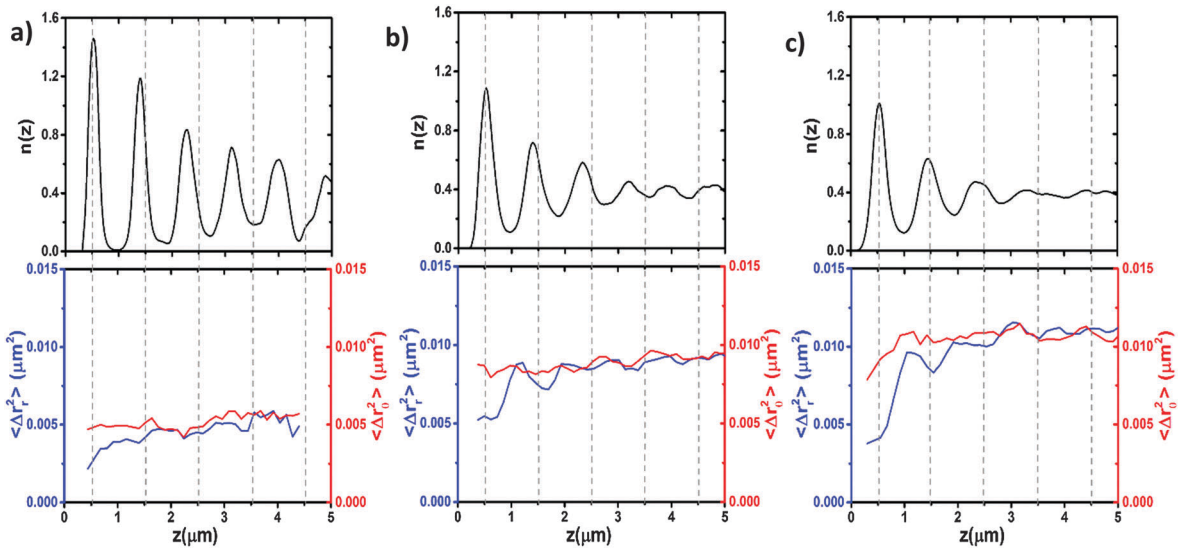

Fig. 9 Radial and azimuthal MSD values (at lagtime 2.0 s, lower graphs) compared to local particle concentrations (upper graph) for the fluid with Φ = 0.39 in the cylinders with R = 5 μm (a), 10 μm (b) and 20 μm (c). Blue and red lines indicate MSDs in the radial and azimuthal directions respectively.

4.2.1. Differences between radial and azimuthal components. We deepen our analysis by decomposing the MSD into the radial and azimuthal directions. From these data, shown in the lower panels of Fig. 9, it becomes evident that strong differences exist between the two components: while the azimuthal MSD only shows a clear z-dependence very close to the wall in the cylinder with R = 20 μm, the radial MSD clearly shows several local minima and maxima in both cylinders. For $z < 1$ μm, the decrease of the radial MSD is much stronger than that of the azimuthal one. This also means that the diffusion becomes strongly anisotropic near the wall. This is in qualitative agreement with the diffusive dynamics of a single particle near a flat wall.[30–32,34,60] For $z >$ 3 μm the radial and azimuthal MSDs become equal; this coincides with the z-range where $n(z)$ becomes nearly constant for R = 10 (Fig. 9b) and 20 μm (Fig. 9c) (it thus appears that as the structure is lost, also the anisotropy of the diffusion disappears). It is also interesting to examine the role of the cylinder radius. As R is decreased from 20 to 10 μm, both MSD components near the wall show less reduction relative to their values in the central region of the cylinder. In case of R = 5 μm (Fig. 9a), effect from the wall becomes significantly weak. This suggests that the increased confinement provides an effect that is similar to the increased hydrodynamic screening when Φ is enhanced. Besides that, a small decrease of the MSD plateaus is found when R is changed from 20 to 10 μm. This illustrates the effect of global confinement.

Interestingly, comparing the z-locations where (especially the radial) MSDs have local minima and maxima with those in the concentration profile $n(z)$, reveal an anti-correlation: 'less crowding' (a lower n) corresponds to a higher 'diffusivity' (a higher MSD). Eral *et al.*[19] measured both number densities and MSDs as a function of distance to the (smooth) wall. They did not report an anti-correlation, but their MSDs were measured in optical planes that were parallel to the walls. This would 'translate' to the azimuthal direction in our experiments, where the anti-correlation is much weaker as compared to the radial direction.

4.2.2. Lagtime dependence. Another interesting aspect of the dynamics concerns the diffusive signature of the local MSD, *i.e.* the lagtime dependence of the MSD for a given z-coordinate. This dependence is generally difficult to measure, since it requires trajectories that are on one hand long enough to obtain a broad range of lagtimes, but on the other hand cover a spatial range that is small enough to allow accurate assignment of a z-location to a trajectory. The combination of our particle size and solvent viscosity, turns out to be ideally suited for our purpose: even at the smallest lag time of 0.03 s, the diffusive displacement is still large enough to be measured (see Fig. 4) while lag times up to 8 s are still small enough to prevent either significant loss of particles from the focal plane, or significant changes in z (the latter can be verified from the MSDs in Fig. 4 by taking the square root).

Analysis of the MSDs at Φ = 0.39 in the cylinder with R = 20 μm revealed that, while the azimuthal MSDs only show a significant change in amplitude very close to the wall (shown in Fig. 9c), and little change in diffusive exponent (data not shown), the time-dependent radial MSD shows strong variations in both magnitude and 'diffusive exponent'. As shown in Fig. 10a, the local particle density oscillates around a 'mean value' that is ultimately reached as z starts to exceed 3 μm. Comparison of the MSD (Fig. 10b) with the local concentration shows that where $n(z)$ has a local maximum, the r-MSD is more strongly subdiffusive, while at local minima of $n(z)$ the r-MSD is more diffusive. After the first 3 peaks, this correlation weakens and the noise level of the MSD increases (due to the smaller area of the ring in the cylinder). For the layer directly adjacent to the wall, the lagtime-dependent r-MSD starts with a (sub) diffusive signature but then reaches a plateau. This indicates that the radial motion is effectively confined to a ring, which in the particular case has a width of $\approx$0.1 particle diameter. This radial confinement aspect, together with the strong anisotropy of the local diffusive displacements, is illustrated (now for a cylinder with R = 5 μm) by Fig. 11.

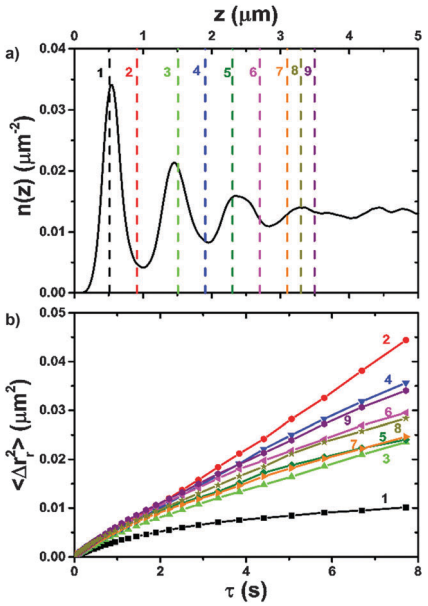

Fig. 10 (a) local number density $n(z)$ of particles as a function of distance from the wall. This data corresponds to $\Phi = 0.39$ inside the largest cylinder (R = 20 μm). (b) MSD in the radial direction as a function of lag time τ. The colors in both panels correspond to each other. Note that the data at τ = 2.0 s are also shown in Fig. 9c.

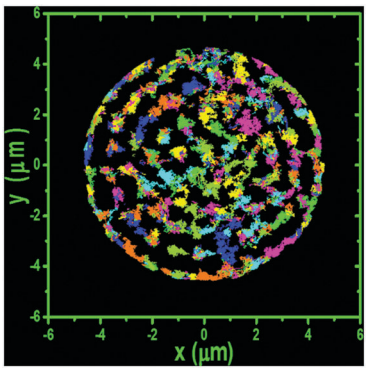

Fig. 11 Two dimensional trajectory plots (*i.e.* time projections of displacements by the same particle) for the fluid with $\Phi = 0.35$ inside a cylinder with R = 5 μm. Integration time is 160 s. Trajectories are identified based on the method described in ref. 50 and 51. Trajectories (1050 tracks) are distinguished *via* their color. Distance units are given in μm.

5. Conclusions

This study both corroborates and extends on earlier findings on the dynamics of confined suspensions. At low concentration we recovered the strong effect of the (most nearby) wall, giving a strong reduction in the diffusion coefficient. Also the global trend that the diffusive dynamics slows down as the confinement length (in our case the cylinder radius) is diminished, was reproduced by our experiments. Several new insights for monodisperse hard sphere fluids were obtained by extending the experiments in microcylinders to a broader range of both cylinder radii and particle volume fractions.

Experiments in the biggest cylinder, approaching the case of a flat wall, allowed to study how both the 'parallel' and the 'perpendicular' diffusion change as the fluid becomes more concentrated. Firstly, the relative reduction in MSD near the wall (as compared to the center of the cylinder) becomes weaker. This is ascribed to a stronger hydrodynamic screening, due to the higher abundance of other particles between the probe and the wall. Secondly, the increase in diffusivity on moving away from the wall is no longer monotonous; local minima and maxima are found to develop as the volume fraction is increased. This phenomenon, which is related to the formation of a layered structures, applies in particular to the radial ('perpendicular') MSD, whose lagtime dependence shows a clear subdiffusive behavior for particles inside layers. Accordingly, the anisotropy in the particle dynamics at the wall is preserved.

For concentrated suspensions, reduction of the cylinder radius has several consequences. Since the effects of local (wall) and global (cylinder) confinement become increasingly intertwined, attribution of the observations to a single cause becomes increasingly difficult. The slow-down of the overall dynamics was also found earlier, and is broadly recognized as a global confinement effect. Our additional observation that the dynamics becomes spatially more homogeneous could be seen as the result of an increased dominance of the global confinement effect. However the fact that this more homogeneous dynamics occurs in spite of a more heterogeneous structure (increased ordering) in the fluid (as show in Fig. 9) is remarkable. It illustrates that the relation between confinement, fluid structure and hydrodynamics is a complex one which still needs to be further understood.

Appendix A

We measured the MSDs for all bulk suspensions as a function of lag time. The MSD at the lowest volume fraction ($\Phi = 0.05$) is close to that of free particle diffusion (solid black line) which reaches a slope of 1 in the log–log plot. MSDs gradually decreases with increasing Φ similar to the previous reports of (nearly) hard sphere systems (Fig. 12).[17,19,52]

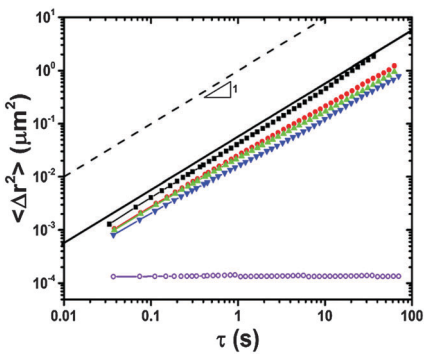

Fig. 12 Mean Squared Displacement (μm^2) *vs.* lag time (s) of colloids in bulk suspension at different volume fractions (Φ): 0.05 (black squares), 0.28 (red circles), 0.35 (green upper triangles), 0.39 (blue lower triangles). Violet open circles indicates the noise floor. Solid black line is the theoretical prediction of Brownian diffusion in similar suspension at infinite dilution. The dashed line has a slope of unity.

Acknowledgements

We thank Dr Dirk van den Ende for discussions and his suggestions. This work was financially supported by NWO-CW (ECHO Grant no. 09.FM.016).

References

1 M. Alcoutlabi and G. B. McKenna, Effects of confinement on material behaviour at the nanometre size scale, *J. Phys.: Condens. Matter*, 2005, **17**(15), R461–R524.
2 V. Teboul and C. A. Simionesco, Properties of a confined molecular glass-forming liquid, *J. Phys.: Condens. Matter*, 2002, **14**(23), 5699–5709.
3 C. L. Jackson and G. B. Mckenna, The Glass-Transition of Organic Liquids Confined to Small Pores, *J. Non-Cryst. Solids*, 1991, **131**, 221–224.
4 P. Scheidler, W. Kob and K. Binder, The relaxation dynamics of a simple glass former confined in a pore, *Europhys. Lett.*, 2000, **52**(3), 277–283.
5 K. Watanabe, T. Kawasaki and H. Tanaka, Structural origin of enhanced slow dynamics near a wall in glass-forming systems, *Nat. Mater.*, 2011, **10**(7), 512–520.
6 T. Fehr and H. Lowen, Glass-Transition in Confined Geometry, *Phys. Rev. E: Stat. Phys., Plasmas, Fluids, Relat. Interdiscip. Top.*, 1995, **52**(4), 4016–4025.
7 G. Hummer, J. C. Rasaiah and J. P. Noworyta, Water conduction through the hydrophobic channel of a carbon nanotube, *Nature*, 2001, **414**(6860), 188–190.
8 M. Muthukumar, Mechanism of DNA transport through pores, *Annu. Rev. Biophys. Biomol. Struct.*, 2007, **36**, 435–450.
9 M. H. G. Duits, S. Ghosh and F. Mugele, Measuring Advection and Diffusion of Colloids in Shear Flow, *Langmuir*, 2015, **31**(21), 5689–5700.
10 S. Ghosh, F. Mugele and M. H. G. Duits, Effects of shear and walls on the diffusion of colloids in microchannels, *Phys. Rev. E: Stat., Nonlinear, Soft Matter Phys.*, 2015, **91**(5), 052305.
11 D. Semwogerere, J. F. Morris and E. R. Weeks, Development of particle migration in pressure-driven flow of a Brownian suspension, *J. Fluid Mech.*, 2007, **581**, 437–451.
12 M. Frank, *et al.*, Particle migration in pressure-driven flow of a Brownian suspension, *J. Fluid Mech.*, 2003, **493**, 363–378.
13 G. M. Whitesides, The origins and the future of microfluidics, *Nature*, 2006, **442**(7101), 368–373.
14 B. Bhushan, J. N. Israelachvili and U. Landman, Nanotribology: friction, wear and lubrication at the atomic scale, *Nature*, 1995, **374**(6523), 607–616.
15 V. N. Michailidou, *et al.*, Dynamics of Concentrated Hard-Sphere Colloids Near a Wall, *Phys. Rev. Lett.*, 2009, **102**(6), 068302.
16 E. V. Russell and N. Israeloff, Direct observation of molecular cooperativity near the glass transition, *Nature*, 2000, **408**(6813), 695–698.
17 W. K. Kegel and A. van Blaaderen, Direct observation of dynamical heterogeneities in colloidal hard-sphere suspensions, *Science*, 2000, **287**(5451), 290–293.
18 P. G. Debenedetti and F. H. Stillinger, Supercooled liquids and the glass transition, *Nature*, 2001, **410**(6825), 259–267.
19 H. B. Eral, *et al.*, Influence of confinement by smooth and rough walls on particle dynamics in dense hard-sphere suspensions, *Phys. Rev. E: Stat., Nonlinear, Soft Matter Phys.*, 2009, **80**(6), 061403.
20 K. V. Edmond, C. R. Nugent and E. R. Weeks, Influence of confinement on dynamical heterogeneities in dense colloidal samples, *Phys. Rev. E: Stat., Nonlinear, Soft Matter Phys.*, 2012, **85**(4), 041401.
21 S. Mandal, *et al.*, Multiple reentrant glass transitions in confined hard-sphere glasses, *Nat. Commun.*, 2014, **5**, 1.
22 Y. Tang, *et al.*, Free-expansion melting of a colloidal monolayer, *Phys. Rev. Lett.*, 1989, **62**(20), 2401.
23 C. R. Nugent, *et al.*, Colloidal Glass Transition Observed in Confinement, *Phys. Rev. Lett.*, 2007, **99**(2), 025702.
24 B. Cui, B. Lin and S. A. Rice, Dynamical heterogeneity in a dense quasi-two-dimensional colloidal liquid, *J. Chem. Phys.*, 2001, **114**(20), 9142–9155.
25 C. Reichhardt and C. O. Reichhardt, Fluctuating topological defects in 2D liquids: Heterogeneous motion and noise, *Phys. Rev. Lett.*, 2003, **90**(9), 095504.
26 S. C. Glotzer, Spatially heterogeneous dynamics in liquids: insights from simulation, *J. Non-Cryst. Solids*, 2000, **274**(1), 342–355.
27 H. Brenner, The slow motion of a sphere through a viscous fluid towards a plane surface, *Chem. Eng. Sci.*, 1961, **16**(3–4), 242–251.
28 R. G. Cox and H. Brenner, The slow motion of a sphere through a viscous fluid towards a plane surface—II Small gap widths, including inertial effects, *Chem. Eng. Sci.*, 1967, **22**(12), 1753–1777.
29 H. B. Eral, *et al.*, Anisotropic and Hindered Diffusion of Colloidal Particles in a Closed Cylinder, *Langmuir*, 2010, **26**(22), 16722–16729.
30 B. Lin, J. Yu and S. A. Rice, Direct measurements of constrained Brownian motion of an isolated sphere between two walls, *Phys. Rev. E: Stat. Phys., Plasmas, Fluids, Relat. Interdiscip. Top.*, 2000, **62**(3), 3909–3919.
31 M. D. Carbajal-Tinoco, R. Lopez-Fernandez and J. L. Arauz-Lara, Asymmetry in Colloidal Diffusion near a Rigid Wall, *Phys. Rev. Lett.*, 2007, **99**(13), 138303.
32 M. A. Bevan and D. C. Prieve, Hindered diffusion of colloidal particles very near to a wall: Revisited, *J. Chem. Phys.*, 2000, **113**(3), 1228–1236.
33 P. Holmqvist, J. K. Dhont and P. R. Lang, Anisotropy of Brownian motion caused only by hydrodynamic interaction with a wall, *Phys. Rev. E: Stat., Nonlinear, Soft Matter Phys.*, 2006, **74**(2), 021402.
34 P. Holmqvist, J. K. G. Dhont and P. R. Lang, Colloidal dynamics near a wall studied by evanescent wave light scattering: Experimental and theoretical improvements and methodological limitations, *J. Chem. Phys.*, 2007, **126**(4), 044707.
35 J. Mittal, *et al.*, Layering and Position-Dependent Diffusive Dynamics of Confined Fluids, *Phys. Rev. Lett.*, 2008, **100**(14), 145901.

36 Z. T. Nemeth and H. Lowen, Freezing and glass transition of hard spheres in cavities, *Phys. Rev. E: Stat. Phys., Plasmas, Fluids, Relat. Interdiscip. Top.*, 1999, **59**(6), 6824–6829.
37 P. P. Lele, *et al.*, Colloidal diffusion and hydrodynamic screening near boundaries, *Soft Matter*, 2011, **7**(15), 6844–6852.
38 V. N. Michailidou, *et al.*, Anisotropic diffusion of concentrated hard-sphere colloids near a hard wall studied by evanescent wave dynamic light scattering, *J. Chem. Phys.*, 2013, **139**(16), 164905.
39 J. W. Swan and J. F. Brady, Anisotropic diffusion in confined colloidal dispersions: The evanescent diffusivity, *J. Chem. Phys.*, 2011, **135**(1), 014701.
40 S. Lang, *et al.*, Glass Transition in Confined Geometry, *Phys. Rev. Lett.*, 2010, **105**(12), 125701.
41 N. Saklayen, *et al.*, Slow dynamics in cylindrically confined colloidal suspensions, *AIP Conf. Proc.*, 2013, **1518**(1), 328–335.
42 G. L. Hunter, K. V. Edmond and E. R. Weeks, Boundary Mobility Controls Glassiness in Confined Colloidal Liquids, *Phys. Rev. Lett.*, 2014, **112**(21), 218302.
43 A. E. Cervantes-Martínez, *et al.*, Colloidal diffusion inside a spherical cell, *Phys. Rev. E: Stat., Nonlinear, Soft Matter Phys.*, 2011, **83**(3), 030402.
44 N. A. M. Verhaegh and A. v. Blaaderen, Dispersions of Rhodamine-Labeled Silica Spheres: Synthesis, Characterization, and Fluorescence Confocal Scanning Laser Microscopy, *Langmuir*, 1994, **10**(5), 1427–1438.
45 V. I. Uricanu and M. H. G. Duits, Micromechanical Behavior of Adhesive Granular Silica Layers: Structure Deformation, *Langmuir*, 2006, **22**(18), 7783–7792.
46 A. Vanblaaderen and A. Vrij, Synthesis and Characterization of Colloidal Dispersions of Fluorescent, Monodisperse Silica Spheres, *Langmuir*, 1992, **8**(12), 2921–2931.
47 W. B. Russel, D. A. Saville and W. R. Schowalter, *Colloidal dispersions*, Cambridge University Press, 1992.
48 S. E. Paulin and B. J. Ackerson, Observation of a Phase-Transition in the Sedimentation-Velocity of Hard-Spheres, *Phys. Rev. Lett.*, 1990, **64**(22), 2663–2666.
49 A. Oláh, H. Hillborg and G. J. Vancso, Hydrophobic recovery of UV/ozone treated poly(dimethylsiloxane): adhesion studies by contact mechanics and mechanism of surface modification, *Appl. Surf. Sci.*, 2005, **239**(3–4), 410–423.
50 J. C. Crocker and D. G. Grier, Methods of Digital Video Microscopy for Colloidal Studies, *J. Colloid Interface Sci.*, 1996, **179**(1), 298–310.
51 E. Weeks, Particle tracking codes http://www.physics.emory.edu/~weeks/idl/index.html.
52 E. R. Weeks, *et al.*, Three-Dimensional Direct Imaging of Structural Relaxation Near the Colloidal Glass Transition, *Science*, 2000, **287**(5453), 627–631.
53 R. Hartkamp, *et al.*, A study of the anisotropy of stress in a fluid confined in a nanochannel, *J. Chem. Phys.*, 2012, **137**(4), 044711.
54 V. Teboul and C. A. Simionesco, Properties of a confined molecular glass-forming liquid, *J. Phys.: Condens. Matter*, 2002, **14**(23), 5699.
55 T. Fehr and H. Löwen, Glass transition in confined geometry, *Phys. Rev. E: Stat. Phys., Plasmas, Fluids, Relat. Interdiscip. Top.*, 1995, **52**(4), 4016.
56 A. J. Archer, P. Hopkins and M. Schmidt, Dynamics in inhomogeneous liquids and glasses via the test particle limit, *Phys. Rev. E: Stat., Nonlinear, Soft Matter Phys.*, 2007, **75**(4), 040501.
57 D. H. Van Winkle and C. Murray, Layering in colloidal fluids near a smooth repulsive wall, *J. Chem. Phys.*, 1988, **89**(6), 3885–3891.
58 S. A. Rice, Structure in confined colloid suspensions, *Chem. Phys. Lett.*, 2009, **479**(1), 1–13.
59 E. Wonder, B. Lin and S. A. Rice, Single-particle diffusion in dense inhomogeneous colloid suspensions in ribbon channels, *Phys. Rev. E: Stat., Nonlinear, Soft Matter Phys.*, 2011, **84**(4), 041403.
60 P. Holmqvist, J. K. G. Dhont and P. R. Lang, Anisotropy of Brownian motion caused only by hydrodynamic interaction with a wall, *Phys. Rev. E: Stat., Nonlinear, Soft Matter Phys.*, 2006, **74**(2), 021402.

